Beta bursts in SMA mediate anticipatory muscle inhibition

Abbreviated title: SMA beta bursts mediate anticipatory inhibition

V. Manyukhina[1], O. Abdoun[1], F. Di Rienzo[1,2], F. Barlaam[1], S. Daligault[3], C. Delpuech[1,3], Maciej Szul[4,5,6], James Bonaiuto[4,5], M. Bonnefond[1]*, C. Schmitz[1]*

*both authors equally contributed to the work

[1]Université Claude Bernard Lyon 1, CNRS, INSERM, Centre de Recherche en Neurosciences de Lyon CRNL U1028 UMR5292, COPHY, F-69500, Bron, France

[2]Université de Lyon, Université Claude Bernard Lyon 1, Laboratoire Interuniversitaire de Biologie de la Motricité-UR 7424, F-69100, Villeurbanne, France

[3]CERMEP-Imagerie du Vivant, MEG Departement, F-69500, Bron, France

[4]Université de Lyon, Université Claude Bernard Lyon 1, F-69100, Villeurbanne, France

[5]Institut des Sciences Cognitives Marc Jeannerod, CNRS, UMR5229, F-69500, Bron, France

[6]Department of Psychiatry and Psychotherapy, Faculty of Medicine, University of Tübingen, 72076 Tübingen, Germany

Corresponding author:

Viktoriya Manyukhina

Université Claude Bernard Lyon 1

43 Bd du 11 Novembre 1918, 69100, Villeurbanne, France

Telephone: +33 7 45678954

Email: vimanyukhina@gmail.com

Keywords: motor inhibition, anticipation, beta bursts, magnetoencephalography (MEG), supplementary motor area (SMA)

Abstract

In motor networks, inhibition has been associated with oscillatory activity in the mu (8-12Hz) or beta (13-30Hz) bands, yet the mechanisms by which they exert influence at the muscular level remain unclear. The Bimanual Load-Lifting Task (BLLT) elicits anticipatory inhibition of the elbow flexors in the load-supporting arm during voluntary load-lifting, providing a suitable model to study oscillatory mechanisms of muscle inhibition. We recorded magnetoencephalography (MEG) in adult participants performing the BLLT. Optimal postural stabilization occurred when *Biceps brachii* inhibition preceded unloading by ~30 ms. Stronger muscle inhibition in this window was associated with reduced excitability, indexed by high-gamma (90-130Hz) power, and increased high-beta power in the contralateral Supplementary Motor Area (SMA), with high-gamma power reduction partially mediating the effect of high-beta power on anticipatory inhibition. Furthermore, trials containing beta bursts (22-28Hz) exhibited optimally timed anticipatory inhibition and a concurrent reduction in high-gamma power. Our data indicate that optimal anticipatory inhibition in the load-supporting elbow flexor is achieved through SMA suppression mediated by inhibitory beta bursts. To our knowledge, these results provide the first evidence that beta bursts can exert direct inhibitory control over muscle function, while advancing understanding of motor anticipation and informing future clinical and developmental studies.

Introduction

Anticipatory postural adjustments (APA) are essential for smooth and coordinated motor behavior, as voluntary movements often cause postural perturbations that must be anticipated and compensated for (Massion, 1992). Yet, the neural mechanisms underlying APA, and particularly the inhibitory regulation of muscle activity they involve, remain poorly understood. The bimanual load-lifting task (BLLT) offers a naturalistic approach to studying APA and their associated inhibitory muscle control in humans (Hugon et al., 1982). In this task, the postural arm supports a load placed on its wrist while the participant lifts it with the other, motor arm. The unloading induces a change in force, causing destabilization of the postural forearm, observed as an upward movement. APA, initiated before the object is lifted, counteract this perturbation and stabilize the posture. A core signature of APA in the BLLT is the inhibition of postural elbow flexors, reflected in reduced electromyographic (EMG) activity. This anticipatory muscle inhibition precedes unloading, contributing to the horizontal stabilization of the forearm during load-lifting and ensuring a smooth transition to a new equilibrium.

While prior research (Ng et al., 2013a) examined the network underlying APA in the BLLT, the specific mechanisms governing anticipatory muscle inhibition, distinct from the subsequent postural stabilization, remain unexplored. A clear EMG signature of muscle inhibition makes the BLLT a valuable framework for exploring the oscillatory mechanisms of motor inhibition, thereby enabling direct investigation of inhibitory control at the muscle level. Accumulated evidence links inhibition in motor networks to mu (8-12 Hz) and beta (13-30 Hz) bands (see below), yet it remains unclear whether such activity directly contributes to inhibitory muscle control. Our first aim was therefore to elucidate this relationship by linking mu and beta activity to muscle inhibition strength and cortical excitability, thereby contributing to a fundamental understanding of how inhibitory control is

implemented in the brain. Our second aim was to explore the neural pathways underlying mature anticipatory muscle inhibition in adults, advancing understanding of the neural basis of motor anticipation and providing a foundation for investigating the development of anticipatory control in children. Although anticipatory inhibition is integral to bimanual coordination, the BLLT allows postural stabilization processes to be studied separately from load-lifting, as APA-related postural control and load-lifting motor control are largely segregated across hemispheres, supported by evidence that lesions contralateral, but not ipsilateral, to the postural forearm reduce APA (Massion, 1992; Viallet et al., 1992).

Motor inhibition has previously been associated with decreased activity in the primary motor cortex (M1; Kazennikov et al., 2005, 2006; Borgomaneri et al., 2020). However, in the BLLT, Ng et al. (2013b) observed more pronounced beta desynchronization preceding unloading in the supplementary motor area (SMA) contralateral to the load-supporting forearm than in M1. They therefore speculated that corticospinal projections originating from the SMA, rather than from M1, may play a central role in APA regulation. To clarify the underlying neural pathway, we investigated whether anticipatory inhibition in the elbow flexors of the load-supporting forearm is associated with reduced activity in the contralateral M1 or SMA and examined the network supporting this inhibition.

Previous studies on the oscillatory mechanisms of motor inhibition have yielded mixed evidence, implicating both mu and beta oscillatory activity in the inhibitory process. Elevated mu power has been associated with motor inhibition, particularly during action withholding and action observation tasks (Bönstrup et al., 2015; Köster and Meyer, 2023). Beta-band activity, predominantly observed in bursts (Lundqvist et al., 2024), has been implicated in the slowing of motor actions during the pre-movement phase (Khanna and Carmena, 2017; Little et al., 2019), and in the inhibition of initiated actions (Picazio et al., 2014; Jana et al., 2020; Schaum et al., 2020). However, the oscillatory mechanisms of anticipatory motor inhibition remain unstudied, leaving it unclear whether alpha- or beta-

band activity mediates this process. Furthermore, whether mu or beta activity can directly mediate inhibition at the final effector stage of motor control – the muscles – and the mechanisms underlying this inhibition have yet to be established. We addressed these questions by examining the mechanisms of anticipatory muscle inhibition in the BLLT.

Methods

Participants

Sixteen right-handed adults without neurological or psychiatric conditions (11 males, mean age 27 ± standard deviation (SD) 3.8 years) participated in this study. Handedness of the participants was determined using the Edinburgh Handedness Inventory (Oldfield, 1971). All participants gave written informed consent in accordance with the Declaration of Helsinki. The study was approved by the local ethics committee (South East IV Committee for the Protection of Persons).

A study involving the same participants, but examining learning mechanisms in a different task during the same experimental session, has previously been published (Di Rienzo et al., 2019). Due to the low variability observed in the behavioral measures in the BLLT, we expected low variability in neural responses, which justified using a smaller sample size, consistent with previous MEG studies on APAs in the BLLT (N=15, Ng et al. (2013a)). As no prior study had specifically estimated the correlation between beta activity and inhibition strength, we based the effect size on a related study by Jana et al. (2020), which reported a correlation of r = 0.66 between beta burst timing and EMG onset in a stop-signal task. Using this effect size, the power analysis indicated that a sample of 12 subjects would be sufficient to achieve 80% power at an alpha level of 0.05 for a one-sided correlation.

Experimental setting and task

The experimental setup of the BLLT, while recording brain activity using EEG (Barlaam et al., 2011) or MEG (Di Rienzo et al., 2019), has been described in more detail elsewhere. In short, while participants were seated under the MEG helmet, their left arm was positioned adjacent to the trunk, with the elbow resting on a support and fixed to allow only upward and downward rotations. They were instructed to maintain the left forearm in a horizontal semi-prone position, as if supporting a tray. This instruction implicitly defined the reference frame to be preserved during lifting. A non-magnetic wristband fitted with a vacuum switch system (30 kN/m^2) strain gauge was worn on the wrist, allowing an 850g load to be placed on top of it (in the voluntary unloading condition), or suspended, with the possibility of being released by 3.5 kN/m^2 air pulses (in the imposed unloading condition).

In the voluntary unloading condition, the participants positioned their right hand above the object to be lifted. Each trial started with a two-second fixation on a light spot projected onto the wrist to limit eye movements during lifting. Upon light extinction (fade-out), participants were instructed to lift the load placed on top of the wristband at any time, raising it up to approximately ten centimeters above the device. After a few seconds of holding the load, participants had to return it to its initial position, completing the trial. Since participants performed the unloading themselves, the use of APA resulted in minimal forearm destabilization, reflected in low elbow rotation, following unloading. In this condition, APA are characterized by anticipatory EMG inhibition in the forearm flexor muscles (*Biceps brachii* and *Brachioradialis*), which typically occurs just before the onset of unloading (Hugon et al., 1982; Barlaam et al., 2011).

In the imposed (control) unloading condition, the experimenter released the load at a random time after light extinction, making the use of APA impossible. In contrast to voluntary unloading, imposed unloading results in a significant passive upward rotation of

the elbow and inhibition of the forearm flexor muscles after unloading onset, known as the unloading reflex (Hugon et al., 1982; Schmitz et al., 2002).

In total, there were 90 trials in both the imposed and voluntary unloading conditions. To reduce fatigue, they were organized into sessions of ten trials each, with intervals of around one minute between the sessions.

Behavioural data acquisition

Detection of load-lifting timing

The onset of load-lifting (unloading, zero reference time point) was automatically identified as the initial deflection in the force signal recorded by the force plate sensor attached to the non-magnetic wristband, using a threshold function in CTF® DataEditor software. The automatically assigned label was then visually inspected and manually corrected if needed.

Elbow-joint rotation

Upward rotation of the elbow joint following load release or lifting was measured across all trials and conditions using a copper potentiometer aligned with the elbow joint axis and sampled at 20 kHz. The signal was resampled at 600 Hz for analysis. The deflection amplitude was recorded in arbitrary units provided by the equipment.

Electromyography

Electromyography (EMG) data were collected at a sampling frequency of 600 Hz using bipolar surface electrodes (2.5 mm² surface area) positioned over the left *Brachioradialis*, *Biceps brachii*, and *Triceps brachii* on the postural side, as well as the right arm *Biceps brachii*. To investigate anticipatory muscle inhibition in this study, we analyzed EMG data from the left *Biceps brachii*, a postural elbow flexor that suppresses activity in anticipation of unloading in the BLLT, as indicated by decreased EMG activity (Massion et al., 1999). Though the left *Brachioradialis* exhibits similar dynamics, being inhibited in the same trials as the *Biceps brachii*, with comparable onset and duration (Barlaam et al., 2011), we focused our analysis on the *Biceps brachii* due to its higher signal-to-noise ratio. Considering their closely matched dynamics, we however suggest that inhibition of both elbow flexors, *Biceps brachii* and *Brachioradialis*, is governed by similar postural control mechanisms.

Behavioural data preprocessing

Elbow rotation

To evaluate postural stabilization as an indicator of APA efficacy in the voluntary unloading condition, we introduced two metrics: Peak Elbow Rotation and Elbow Rotation Decline, representing the two principal directions of forearm destabilization (see Fig. 2A, left panel). We assumed that in trials when APA are effective, both Peak Elbow Rotation and Elbow Rotation Decline would exhibit values close to zero, indicating optimal postural stabilization.

To estimate Peak Elbow Rotation and Elbow Rotation Decline in the voluntary unloading condition, the time point of maximal elbow deflection was visually identified in the time series using the ‘annotations’ tool in MNE-Python. This step was performed

manually because, in most trials, peak elbow rotation was too small to be reliably detected with automatic algorithms. The time series were then epoched from -1.7 to 1.2 s relative to the annotated peak of elbow deflection. Peak Elbow Rotation was computed as the average of baseline-corrected values around the point of maximal deflection. Elbow Rotation Decline was computed automatically as the average of baseline-corrected minimum values preceding the maximal elbow deflection (see Supplementary Materials for details on the time intervals used).

Elbow Rotation Decline and Peak Elbow Rotation were calculated individually for each trial, followed by visual inspection of the time intervals used for their calculation (see examples in Supplementary Fig. S1). For demonstration purposes, Figure 1B shows the resulting amplitudes of Peak Elbow Rotation and Elbow Rotation Decline in three example trials. Trials containing severe artifacts that precluded reliable estimation of elbow rotation measures were identified and excluded. The number of such trials per participant ranged from 0 to 5 (mean = 1.25, SD = 1.39). All analyses involving elbow rotation data were conducted on the remaining artifact-free trials.

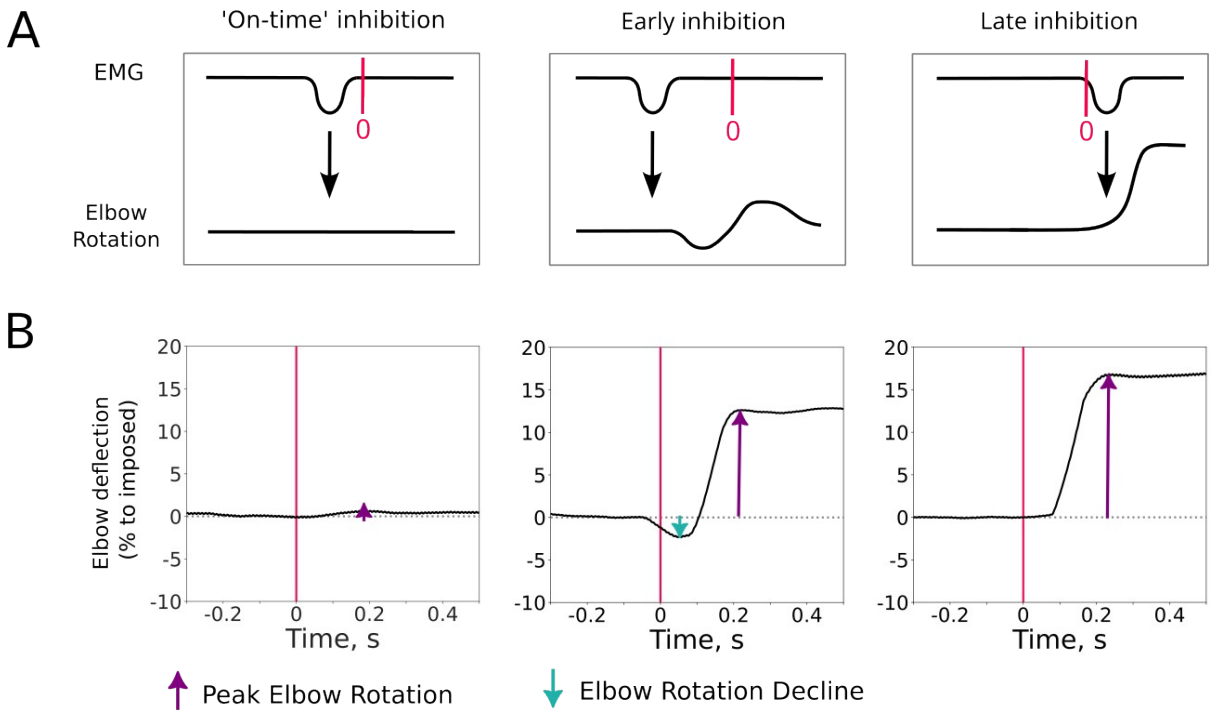

Figure 1. Estimation of elbow deflection parameters and their expected relationship with *Biceps brachii* inhibition timing. **A:** Schematic illustration of three primary possible scenarios for *Biceps brachii* inhibition timing and its hypothetical impact on elbow rotation. See Methods (*Estimation of the EMG inhibition* section) for details. **B:** Single-trial examples aligned to unloading onset (time = 0), schematically illustrating the amplitudes of Peak Elbow Rotation and Elbow Rotation Decline. Values are presented as percentages of elbow deflection during voluntary unloading relative to the individual maximum, estimated as the median peak elbow rotation in the imposed condition.

In the imposed condition, to assess the postural destabilization triggered by the experimenter's unexpected release of the load, only upward elbow rotation was measured, as a decrease in elbow rotation was not observed in this condition. Peak Elbow Rotation was defined as in the voluntary condition, except that the prominent peak allowed automatic detection of maximal elbow deflection within the trial window.

Electromyography (EMG)

For this study, we analysed EMG recordings from the left *Biceps brachii*. Preprocessing followed established protocols (Schmitz et al., 2002; Barlaam et al., 2011, 2018) and included epoching from -1 to 0.5 s relative to the onset of unloading, mean subtraction, and band-pass filtering using a finite impulse response (FIR) filter with a Hamming window in the 25-150 Hz range, chosen after inspecting group-averaged muscle power spectral density. The filtered signals were then rectified to enable visualization of *Biceps brachii* inhibition as a reduction in EMG power (see Fig. 2A, right panel). After log10-transformation and baseline correction (-1 to -0.5 s), the EMG signal was smoothed using a 30 ms moving average with 33% overlap to improve the reliability of inhibition estimates.

Estimation of the EMG inhibition

Since high noise levels in the EMG signal prevented accurate trial-by-trial assessment of muscle inhibition, we instead aimed to quantify inhibition strength during the period when it most effectively contributed to subsequent postural stabilization – specifically, when inhibition was followed by the maintenance of a stable horizontal forearm position. This involved identifying the time interval in which *Biceps brachii* inhibition had the strongest effect on both Elbow Rotation Decline and Peak Elbow Rotation, bringing both values close to zero and indicating a stabilized posture.

The anticipatory muscle inhibition observed in this paradigm likely reflects the suppression, or adjustment, of the ongoing postural command responsible for elbow flexor control during load support, finely tuned to maintain the forearm in a horizontal position despite the loss of opposing force due to load release. Its effectiveness depends critically on timing, which must be optimal: not too early, to ensure forearm stability until the load is released, and not too late, to prevent destabilization caused by the sudden change in force. Figure 1A provides a schematic overview of these three timing scenarios: early, on-time, and late *Biceps brachii* inhibition, along with their expected behavioural effects.

To investigate the mechanisms underlying the most efficient strategy, i.e., on-time inhibition, which is predominant in adult participants (Schmitz et al., 2002), we aimed to determine the time at which muscle inhibition results in the smallest negative elbow deflection (Elbow Rotation Decline) and lowest Peak Elbow Rotation.

To this end, we fitted linear regression models for each participant across trials, using Elbow Rotation Decline and Peak Elbow Rotation as predictors of *Biceps brachii* EMG. The OLS() function from the statsmodels.regression.linear_model module (statsmodels library, v. 0.14.1) was used to fit a separate linear regression model at each time point of the smoothed

EMG signal (see above). The F-value was used as the evaluation metric for each regression model, and the coefficient of determination (R^2) was used to assess the quality of the prediction. F-values were log10-transformed to normalize their distribution and baseline-corrected (-1 to -0.5 s). Therefore, positive baseline-corrected F-values indicated time intervals where Elbow Rotation Decline and Peak Elbow Rotation predicted *Biceps brachii* EMG more strongly than its baseline activity. A one-sample permutation cluster test was used to assess whether the positive, baseline-corrected F-values significantly differed from zero across subjects, within the time interval of -0.25 to 0.1 s relative to unloading.

In the imposed condition, where anticipating load release was impossible, the unloading reflex – characterized by *Biceps brachii* inhibition – occurred approximately 100 ms after unloading. To detect muscle activity decrease in each participant, EMG data were preprocessed following the same steps as in the voluntary condition and baseline-corrected (-1 to -0.5 s). For each participant, EMG inhibition strength was calculated by averaging the signal within a 30 ms window centered on the latency of maximal inhibition in the trial-averaged data.

MRI data acquisition and preprocessing

Structural magnetic resonance imaging (MRI; voxel size 0.9 mm x 0.9 mm x 0.9 mm; TR=3500 ms, TE=2.24 ms) data were obtained from all participants using a 3T Siemens Magnetom scanner (CERMEP, France - MAGNETOM Prisma, Siemens HealthCare). T1-weighted images were preprocessed with the ‘recon-all’ procedure from FreeSurfer software (version 6.0.0; Fischl et al., 2002), which includes motion correction, intensity normalization, removal of non-brain tissue, cortical surface reconstruction, and subcortical segmentation.

The cortical surface was parcellated into 450 regions using the ‘HCPMMP1’ atlas (Glasser et al., 2016), as implemented in MNE-Python software (v. 1.7.0; Gramfort et al., 2013). Source-level MEG analysis was then restricted to brain regions previously associated with voluntary unloading in the BLLT task (Schmitz et al., 2005; Ng et al., 2011, 2013a, 2013b). To investigate anticipatory inhibition mechanisms, our analysis specifically targeted the right-hemisphere network, contralateral to the load-supporting arm, where inhibition occurs. Although anticipatory inhibition is inherently linked to bimanual coordination in the BLLT, focusing on the right-hemispheric network allowed us to investigate the pathways directly implicated in postural *Biceps brachii* inhibition and APA, which primarily rely on the hemisphere contralateral to the postural forearm (Massion, 1992; Viallet et al., 1992). A full list of the regions of interest is provided in Supplementary Table S1.

In addition to cortical regions, several subcortical structures in the right hemisphere implicated in the BLLT task were included in the MEG source-level analysis. These regions were automatically parcellated using the Aseg atlas in FreeSurfer and included the cerebellar cortex and basal ganglia (caudate nucleus, putamen, and globus pallidus).

MEG data acquisition

Magnetoencephalography (MEG) recordings were acquired using a CTF-MEG system (CERMEP, France - CTF MEG Neuro Innovations, Inc), equipped with 275 radial gradiometers positioned to cover the scalp, along with 29 reference channels for correcting ambient noise. The MEG signals were digitized at a 600 Hz sampling rate and low-pass filtered between 0 and 150 Hz. Head position was tracked continuously using three coils placed on the nasion and preauricular points before recording.

MEG sensor-level data analysis

Preprocessing steps

MEG data preprocessing and analysis were performed using MNE-python software (v. 1.7.0; Gramfort et al., 2013). Raw MEG data from the voluntary unloading condition (three sessions per participant), aligned to the initial head position within each session, were concatenated. Visual inspection confirmed that head movements did not exceed 1 cm along the x, y, or z axes. A detailed analysis further showed that head position remained stable across all three coordinates during the anticipatory period (-0.5 to 0 s relative to unloading), which was used in subsequent analyses.

The data were high-pass filtered at 1 Hz before applying Independent Component Analysis (ICA) using the ICA() function (number of components: 70, method: 'picard', maximum number of iterations: 1000, reference channels were included in the IC estimation). Components reflecting biological artifacts (blinks, heartbeat, muscle activity) were identified and excluded based on visual inspection of their time courses and topographies. To detect components contaminated by intermittent environmental noise, the find_bads_ref() function (threshold=1.5) was applied to the MEG reference channels. Identified components were then removed from the unfiltered copy of the raw data. The average number of excluded components (mean ± SD) was as follows: EOG-related: 2.06 ± 0.24; ECG-related: 1.25 ± 0.56; EMG-related: 1.44 ± 1.54; artifact noise: 6.56 ± 3.46.

The raw data were epoched from -1.7 to 1.2 s relative to unloading onset. Only trials in which the unloading onset was detectable and the elbow rotation signal did not exhibit severe artifacts were retained for further analysis (number of dropped trials per subject, mean ± SD: 1.19 ± 1.18). Data of 275 axial gradiometers were selected for the analysis. Epochs

were visually inspected and those contaminated by instrumental noise and myogenic artifacts were excluded (number of dropped trials per subject, mean ± SD: 2.00 ± 2.89). Several trials were additionally excluded from the elbow rotation analyses due to the presence of artifacts in time intervals critical for reliably estimating Peak Elbow Rotation and/or Elbow Rotation Decline (see above). The final average number of trials per participant was 86.94 ± 2.97 (mean ± SD).

For the imposed (control) condition, preprocessing included the same steps, with epoching performed in the time interval of -0.5 to 0.5 s relative to unloading onset, resulting in a total of 87.00 ± 5.55 (mean ± SD) trials per subject.

MEG source-level data analysis

Individual brain models and inverse solution

Three MRI-visible fiducial landmarks (nasion, left auricular, and right auricular) were manually positioned and used to define the head coordinate system. Individual structural MRI data were coregistered with the MEG raw data using the mne.gui.coregistration() tool. A single-layer boundary element model (BEM) was created with 20,484 vertices across both hemispheres. A mixed source space was defined, combining a surface-based source space with 'ico4' spacing yielding 5,124 cortical vertices in both hemispheres and a volume source space with 5 mm spacing, which included the cerebellum and basal ganglia comprising a total of 1,300 sources. The forward solution was computed for sources with a minimal distance of 5 mm from the inner skull surface.

Notch filters at 50 and 100 Hz were applied to the raw data after ICA to reduce powerline noise. The data were then band-pass filtered at 25-150 Hz for gamma activity analysis, 1-90 Hz for alpha-beta power analysis, and 1-150 Hz for alpha-beta vs. gamma correlation using zero-phase FIR filters with a Hamming window. The filter length was set to 'auto' with the 'firwin' design and 'reflect_limited' padding. The resulting data were epoched as described in the preprocessing step, and bad trials were excluded based on prior annotations.

The data rank was computed from the epoched data, with a singular value tolerance of 1e-6 applied relative to the largest singular value. The data covariance matrix was then calculated using this rank with the 'empirical' method for the time interval from -1 to 0.1 s relative to unloading onset to capture the brain response associated with anticipatory motor control. Since only gradiometer channels were used and the beamformer approach was adopted, noise covariance estimation for source reconstruction was not necessary. A unit-gain Linearly Constrained Minimum Variance (LCMV) beamformer spatial filter was computed to optimize power orientation, with a regularization coefficient of 0.05 and enabling the rank reduction. The resulting filter was applied to each epoch individually.

Time-frequency analysis

Time-frequency analysis was performed over the full time window from -1.7 to 1.2 s, with symmetric padding of 0.5 s added on both sides of the time array. The resulting data were then cropped to the window of interest (-0.5 to 0.25 s) relative to unloading.

For gamma power estimation, the Multitaper method (using the tfr_array_multitaper() function) was applied to the time series of individual-trial source activity reconstructed with the LCMV beamformer. The analysis was conducted in the 90-130 Hz frequency range, using 7 cycles, a time_bandwidth parameter of 4, and a frequency resolution of 1 Hz. The resulting

power estimates were log10-transformed and averaged across the frequency dimension to yield a mean high-gamma power estimate for the 90-130 Hz band.

For power estimation in the alpha-beta range, the adaptive Superlets algorithm was used (https://github.com/irhum/superlets; Moca et al., 2021). For each trial and brain source, power was estimated in the 1-80 Hz frequency range (base cycle = 3, orders 1-20). Periodic power was then extracted per trial and source using the Specparam tool ('FOOOF'; Donoghue et al., 2020) as the difference between total power and the aperiodic fit, derived from trial-averaged spectra in 2-80 Hz, which was selected based on visual inspection of spectral densities. For further analysis, the 8-30 Hz alpha-beta band was extracted.

Correlational analyses

Previous studies suggest that anticipatory elbow flexor inhibition during voluntary unloading may be attributed to reduced excitability, rather than enhanced inhibitory drive, in the brain regions governing muscle control (Kazennikov et al., 2005, 2006). To test this, we used Spearman's rank correlation to relate our anticipatory inhibition estimate – EMG inhibition (see Results, *Behavioural data* section) – to high-gamma power over time, averaged in the 90-130 Hz band, used as a proxy for cortical excitability. High-gamma activity – typically defined as neural activity within a broad frequency range above 60 or 80 Hz – has been shown to correlate closely with neuronal spiking in both sensory (Ray et al., 2008; Ray and Maunsell, 2011; Suffczynski et al., 2014) and motor networks (Yazdan-Shahmorad et al., 2013), supporting its use as an indicator of regional excitability. Correlations were computed at each time point between -0.25 and 0 s relative to unloading and for each cortical source within the right anticipatory motor network (see Supplementary Table S1). A one-tailed, one-sample permutation cluster test was used to assess whether stronger EMG inhibition is linked to reduced neural activity in the selected network.

To investigate the potential involvement of additional brain regions in the regulation of anticipatory muscle inhibition via alpha- and beta-band synchrony, we computed Spearman's rank correlations between periodic power and EMG inhibition at each source vertex within the right anticipatory motor network, across time-frequency points in the 8-30 Hz range and the -0.25 to 0 s time window. To further assess the contribution of subcortical structures, the same correlation analysis was performed for the right cerebellum and basal ganglia. Separate one-tailed, one-sample permutation cluster tests were conducted to determine whether stronger EMG inhibition was associated with increased alpha- and beta-band power across both the right anticipatory motor network and the subcortical structures.

To assess the relationship between alpha-beta (8-30 Hz) and high-gamma (90-130 Hz) power within the selected SMA cluster region – while controlling for their shared variance due to broadband power fluctuations – we computed partial Spearman's correlation coefficients at each vertex using the partial_corr() function from Pingouin (v. 0.5.3), with mean total power in the 1-130 Hz range included as a covariate (Spaak et al., 2012). The resulting correlation coefficients were then averaged across cluster vertices. Although this approach has certain limitations, it allowed us to account for trial-to-trial power variability common to both frequency bands when estimating their relationship.

Mediation analysis

To further investigate the interplay between high-gamma power, periodic beta power, and EMG inhibition in the SMA cluster region where significant correlations among these measures were observed (see Results, *MEG data* section), we performed a mediation analysis. Specifically, we tested whether high-gamma power (mediator, M) mediated the relationship between beta power (independent variable, X) and EMG inhibition (dependent variable, Y). The analysis focused on the 'peak vertex' within the SMA cluster region,

defined as the vertex showing the strongest correlation between high-gamma power and EMG inhibition. Total (without aperiodic component subtraction) beta and high-gamma power were averaged over their respective frequency bands – 24-25 Hz for beta and 90-130 Hz for gamma – and across the time interval in which a significant correlation between gamma power and EMG inhibition was observed (-0.06 to -0.018 s relative to unloading). Notably, this time window overlapped with the interval during which beta power (24-25 Hz) was correlated with EMG inhibition (see Fig. 3B). The use of a unique time interval for estimation of both the independent variable and the mediator is justified by the fast conduction velocity of neural signals (less than 1 ms), which is below the time resolution of the current data, making it impossible to differentiate their exact timings. Before fitting the models, beta power was adjusted by regressing out (LinearRegression() function, 'sklearn', v. 1.4.2) the total power averaged across a broad frequency range (1-130 Hz) to mimic the partial correlation approach used for the beta power vs. gamma power correlation (see above). The resulting beta and gamma powers were further scaled across subjects to yield standardized mediation parameters.

The mediation analysis employed bootstrapping with 10,000 permutations to obtain robust estimates of the mediation effects. To account for random effects, generalized additive models (GAMs) with linear fixed effects (gamma power, beta power) and random effects per subject (random intercepts, random gamma and beta slopes) were fitted using restricted maximum likelihood (REML). The models used as inputs for the mediation analysis – models A and C' – are described in Table 1. To justify the presence of relationships between the mediator and dependent variable, and between the independent and dependent variables, two additional models – models B and C (Table 1) – were specified. Details justifying the models' linearity assumptions are provided in the Supplementary Methods.

Model	Relationship	Formula (mgcv)
A	$X \rightarrow M$	Gamma ~ Beta+s(Subject,bs='re')+s(Subject,Beta,bs='re')
C’	$X + M \rightarrow Y$	Inhibition ~ Beta+Gamma+s(Subject,bs='re')
		+s(Subject,Beta,bs='re')+s(Subject,Gamma,bs='re')
B	$M \rightarrow Y$	Inhibition ~ Gamma+s(Subject,bs='re')+s(Subject,Gamma,bs='re')
C	$X \rightarrow Y$	Inhibition ~ Beta+s(Subject,bs='re')+s(Subject,Beta,bs='re')

Table 1. Mediation analysis models.

Inhibition: EMG inhibition; *Gamma:* gamma power averaged over 90-130 Hz; *Beta:* adjusted beta power averaged over 24-25 Hz; *s(Subject,bs='re'):* subject-based random intercept; *s(Subject,Beta,bs='re'):* subject-specific random slope for beta power; *s(Subject,Gamma,bs='re'):* subject-specific random slope for gamma power.

Beta bursts extraction

To extract beta bursts at the vertices of interest, we employed the burst detection pipeline developed by Szul et al. (2023; https://github.com/danclab/burst_detection). Time-frequency decomposition and aperiodic component extraction were performed using Superlets and Specparam, respectively, as described above (see *Time-frequency analysis* section*)*. Unlike previous steps, a frequency resolution of 0.25 Hz was employed in the Superlet analysis to improve burst detection accuracy. Beta bursts were detected in the 10-33 Hz frequency band within a -0.8 to 0.4 s window, relative to unloading. To verify the accuracy of burst extraction, trial-wise time-frequency representations with identified bursts were visually inspected.

Bursts were extracted for each trial from the ‘peak vertex’ within the SMA cluster region (see Results, *MEG data* section), identified as showing the strongest correlation

between gamma power and EMG inhibition. For this vertex, only bursts with a burst center frequency between 22-28 Hz and a burst center time between -0.077 and -0.018 s were considered for analysis. These time and frequency intervals were defined based on the observed correlation between beta power and EMG inhibition (Fig. 3B): the time window captured its temporal effect around inhibition, and the frequency range (25 ± 3 Hz) targeted the correlation peak at 25 Hz while accounting for potential variability in burst frequency estimates (see Results, *Beta burst analysis* section, for details on range selection).

Beta bursts analysis

To examine whether trials containing beta bursts within the selected time and frequency range also exhibit more pronounced anticipatory *Biceps brachii* inhibition, we averaged baseline-corrected EMG power time courses across these trials. A one-tailed, one-sample permutation cluster test was conducted across participants within the -0.25 to 0.05 s window relative to unloading to assess whether EMG power was significantly reduced during beta burst trials, indicating stronger anticipatory inhibition.

For further analysis, trials containing beta bursts were aligned to the center time of each burst. For the control trials, an equal number of no-burst trials were selected based on the lowest beta power within the time-frequency range used for burst extraction. These control trials were then aligned to the burst center times from burst trials, ensuring time shuffling in the control condition as well.

To test whether the occurrence of beta bursts was linked to high-gamma power suppression, we compared high-gamma (90-130 Hz) power between trials with bursts and no-burst control trials. A one-tailed, one-sample permutation cluster test (-0.05 to 0.05 s around burst centers, 90-130 Hz) was conducted to assess whether high-gamma power decreased in burst trials compared to no-burst trials.

As a complementary analysis, we investigated the right-hemispheric network supporting anticipatory inhibition. Given that estimating reliable connectivity in burst-like signals is controversial (Lundqvist et al., 2024), the connectivity analysis was performed on extracted beta bursts. Because this analysis was secondary to the main objectives of the study and subject to specific limitations, details of the analysis and results are provided in the Supplementary Materials.

Statistical analysis

Mediation analysis was performed in R (version 4.5.0) using the mediate() function (‘mediation’ package, v. 4.5.0) and the bam() function to fit GAMs (‘mgcv’ package, v. 1.9.0). To check the assumptions of linear regression models, several diagnostic tests were performed. Normality of residuals was assessed with the Shapiro-Wilk test (shapiro(), scipy.stats v. 1.7.3), and autocorrelation was checked using the Durbin-Watson test (durbin_watson(), statsmodels.stats.stattools v. 0.13.5). Homoscedasticity was assessed with the Breusch-Pagan test (het_breuschpagan(), statsmodels.stats.api v. 0.13.5), and multicollinearity with the Variance Inflation Factor (variance_inflation_factor(), statsmodels.stats.outliers_influence v. 0.13.5).

To assess the relationship between neural activity and behavioural parameters at individual time, frequency, and spatial points, we calculated Spearman’s rank correlation coefficient (spearmanr() function, scipy.stats, v. 1.7.3). Spearman’s correlation was chosen due to the potential presence of non-linear relationships between the pairs of variables studied.

To perform cluster analysis, group-level statistics, or to select a common set of vertices across all subjects (e.g., the SMA cluster region or the right anticipatory motor

network), timecourses or correlation coefficients computed for individual brain models were morphed to the template brain, ‘fsaverage’, using the compute_source_morph() function in MNE-Python. For ‘fsaverage’, the BEM and source spaces were created using the same parameters as those applied to the sample data.

A non-parametric permutation cluster one-sample t-test was used for all cluster-level analyses, employing either permutation_cluster_1samp_test() for time-only data or spatio_temporal_cluster_1samp_test() for analyses involving spatial or frequency dimensions as well, with 1,024 permutations used to build a null distribution for cluster-level inference. To stabilize t-statistics in the presence of low variance, the ‘hat’ variance regularization was used. Clusters were formed based on adjacency in time, space, frequency, or their combinations. One- or two-tailed tests were applied depending on the hypotheses, as specified for each test in Methods. Threshold-Free Cluster Enhancement (TFCE) was used for one- or two-dimensional data (time or time-frequency; starting value: 0, step size: 0.2). For higher-dimensional data involving spatial adjacency, a cluster-forming threshold based on $p = 0.001$ was used to manage computational costs. We confirmed the reliability of this approach by comparing TFCE and cluster-based thresholding in a high-gamma-to-EMG inhibition correlation, which yielded similar clusters ($p < 0.05$) across time and within the anticipatory motor network for both methods.

Results

Behavioural data

The group-averaged elbow rotation and EMG modulation over time, including between-subject variability, are presented in Figure 2A. Distributions of Peak Elbow Rotation and Elbow Rotation Decline across trials were significantly non-normal for all participants (Shapiro-Wilk test, $p < 0.05$). Furthermore, for both parameters, the means and SDs were low relative to each participant's maximal elbow rotation in the imposed condition. The average ratio of voluntary to imposed elbow deflection was: Peak Elbow Rotation, 5.46 ± 7.44%; Elbow Rotation Decline, -0.43 ± 2.04% (see Fig. 2B for individual variability). Notably, the observed 5% voluntary Peak Elbow Rotation deflection closely matches earlier findings of 8% in adults (Barlaam et al., 2012), consistent with mature anticipatory control mechanisms stabilizing forearm during voluntary load-lifting.

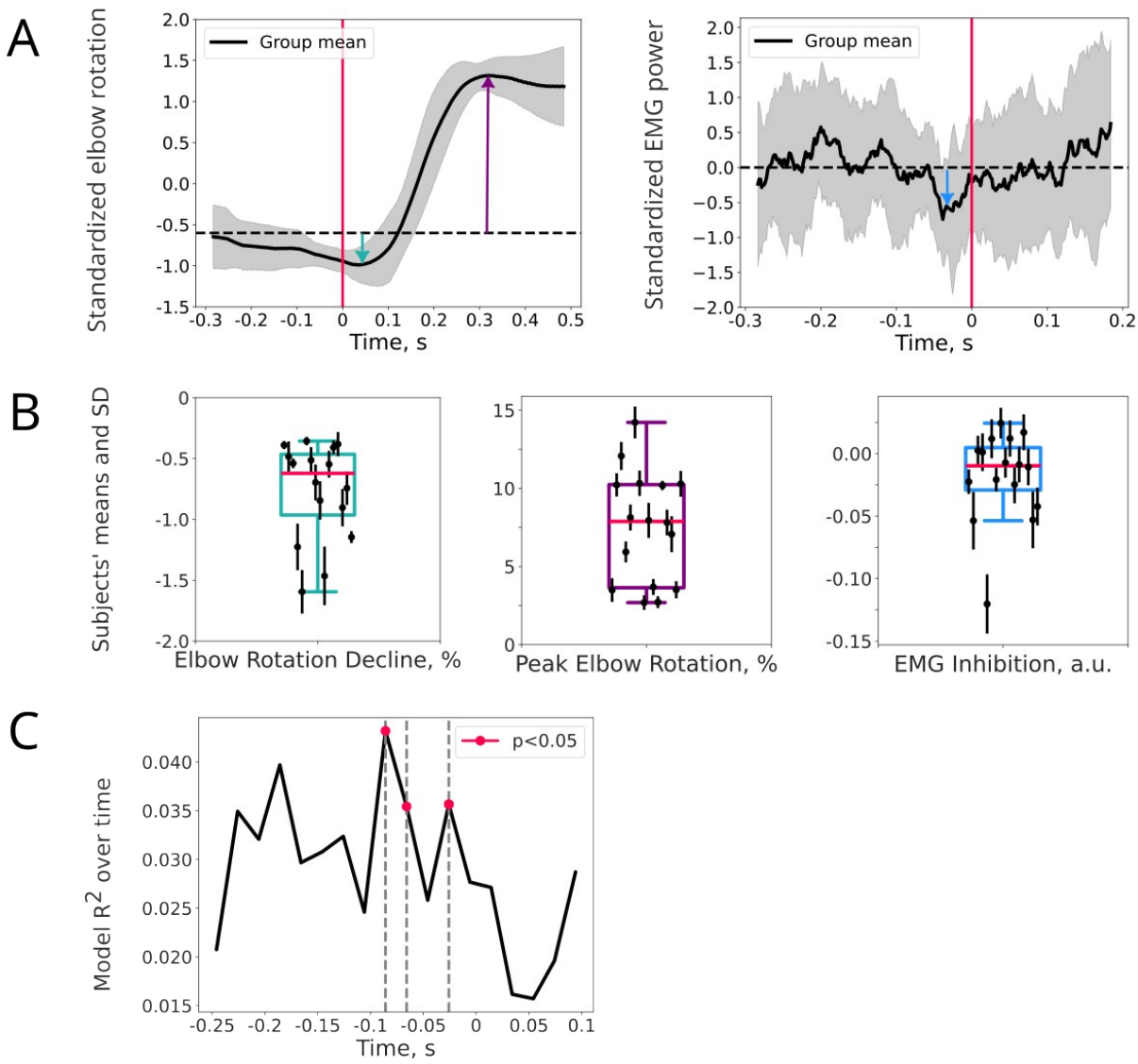

Figure 2. Behavioural analysis results. Data in panels **A** and **C** are aligned to unloading onset (time = 0). **A:** Standardized elbow rotation and *Biceps brachii* EMG. Group means (black line) and SD (gray shading) are shown, with colored arrows indicating the amplitudes of behavioural measures: Elbow Rotation Decline (green), Peak Elbow Rotation (purple), and EMG inhibition (blue). **B:** Participant-wise mean (dots) and SD (whiskers) values for each measure, with boxplots indicating between-subject variability. The red line marks the median, box edges show quartiles (Q1 and Q3), and whiskers extend to 1.5 times the interquartile range. **C:** Group-averaged R^2 values from linear regression models computed at each time point (dependent variable: EMG power; independent variables: Peak Elbow Rotation, Elbow

Rotation Decline). Red markers and gray dashed lines denote time points where the relationship between EMG inhibition and elbow rotation parameters reached significance.

Using within-participant variability in elbow deflection across trials, we aimed to determine the timing of anticipatory inhibition in the *Biceps brachii* that would optimize forearm stabilization. We assumed that optimal elbow flexor inhibition timing would minimize deviations from zero in both Peak Elbow Rotation and Elbow Rotation Decline (‘On-time’ inhibition scenario, Fig. 1A). Optimal inhibition timing was identified by fitting linear regression models predicting *Biceps brachii* EMG from trial-level variability in Peak Elbow Rotation and Elbow Rotation Decline (see Methods, *Estimation of the EMG inhibition* section). Verification of the linearity assumptions for these models is provided in the Supplementary Materials. A permutation cluster test identified significant differences in baseline-corrected F-values, with the strongest effect at three time points: -0.086 s ($t = 4.04$, $p = 0.002$) , -0.066 s ($t = 2.64$, $p = 0.019$), and -0.026 s ($t = 3.9$, $p = 0.022$) relative to unloading, indicating periods when EMG modulation was most strongly associated with elbow rotation. Group-averaged R^2 values for these models are shown in Figure 2C, highlighting these three key intervals. A closer examination of the correlation coefficients between EMG power and the two elbow rotation metrics (see Supplementary Results, Fig. S2) revealed that only around -0.026 s was a stronger EMG suppression associated with both reduced (less negative) Elbow Rotation Decline and lower (less positive) Peak Elbow Rotation, indicative of a more stabilized forearm. The time interval around 26 ms before unloading was therefore consistent with the ‘on-time’ inhibition scenario (Fig. 1A) and corresponded to a clear reduction in group-averaged EMG activity relative to baseline (Fig. 2A, right panel). By contrast, earlier intervals around 86 ms and 66 ms before unloading showed positive associations between EMG and Elbow Rotation Decline, consistent with the ‘early inhibition’ scenario (Fig. 1A) and suggesting that greater Elbow Rotation Decline may

reflect premature anticipatory inhibition. Supporting this interpretation, no forearm lowering was observed in the imposed condition, where anticipatory adjustments could not occur.

The time interval around 26 ms before unloading was therefore identified as the optimal window for *Biceps brachii* inhibition during the voluntary unloading task. Notably, this interval aligns with prior BLLT studies, which indicate that efficient anticipatory postural control is associated with inhibition occurring within 50 ms before unloading onset (Viallet et al., 1987). The 'on-time' *Biceps brachii* inhibition measure, hereafter referred to as EMG inhibition, was calculated as the average of preprocessed (see Methods) and baseline-corrected (-1 to -0.5 s) *Biceps brachii* EMG power within a 30 ms window centered around 26 ms before unloading. Therefore, in individual trials stronger EMG inhibition (more negative values) reflects not only greater inhibition strength but also optimal inhibition timing, whereas weaker EMG inhibition (more positive values) suggests that the actual inhibition occurred either too early or too late.

In contrast to the elbow rotation parameters, EMG inhibition values were more normally distributed (Shapiro-Wilk test, $p > 0.05$ in 14 of 16 participants) and exhibited greater variability across trials within participants (mean ± SD: -0.018 ± 0.034; see Fig. 2B).

MEG data

Correlation of EMG Inhibition with contralateral anticipatory motor network dynamics

To test whether anticipatory inhibition in the *Biceps brachii* is associated with decreased excitability in a cortical region controlling the muscle, we conducted a one-sample permutation cluster test against zero on the correlations between high-gamma power (averaged over 90-130 Hz) – used as a proxy for regional excitability (Murthy and Fetz,

1996; Ray et al., 2008; Lundqvist et al., 2016; Riehle et al., 2018; Brazhnik et al., 2021) – and EMG inhibition, across vertices of the right anticipatory motor network (see Supplementary Table S1). The analysis, conducted within the -0.25 to 0 s interval relative to unloading, revealed a significant correlation effect, peaking in the medial frontal cortex, specifically in the SMA (Fig. 3A), with the cluster spanning from -0.06 to -0.018 s (t_{max} = 6.41, p = 0.039, corrected). This finding suggests that stronger EMG inhibition around 26 ms before unloading is associated with a preceding reduction in high-gamma activity in the medial SMA, with a latency roughly consistent with previously reported SMA-to-muscle neural conduction latencies (Spieser et al., 2013; Entakli et al., 2014).

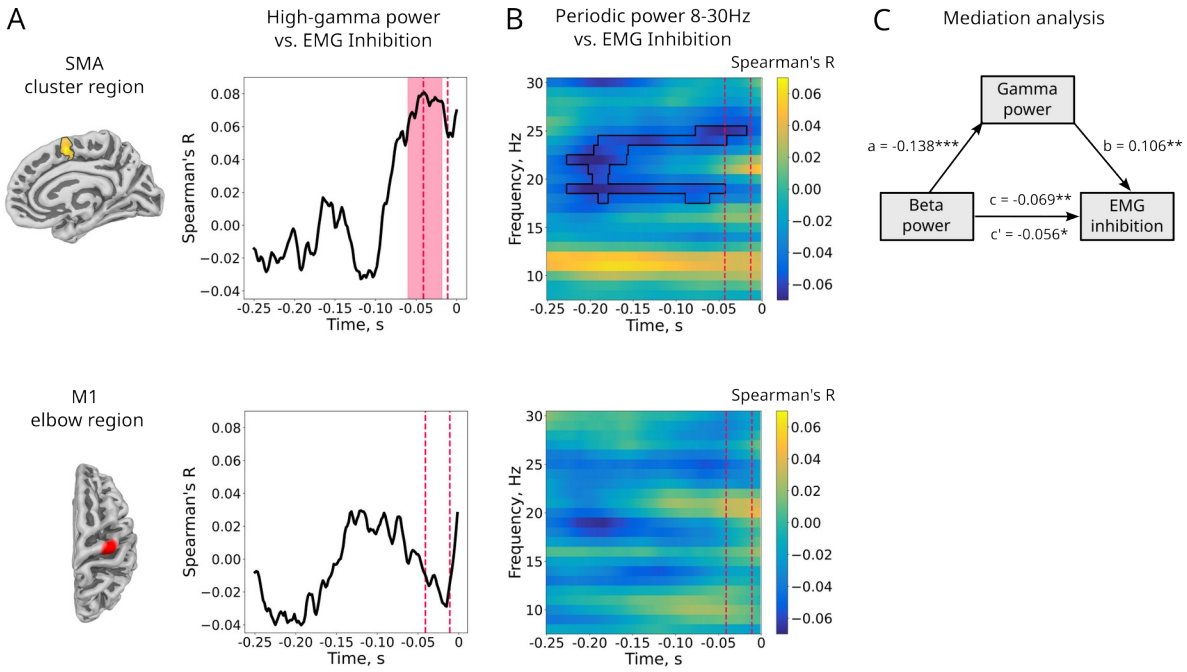

Figure 3. Neural correlates of EMG inhibition and mediation analysis. Data in panels **A** and **B** are aligned to unloading onset (time = 0). **A:** *Upper panel:* A cluster-level significant correlation effect between high-gamma power (90-130 Hz) and EMG inhibition (30 ms window centered on -0.026 s, indicated by red dashed lines) with the strongest effect observed in the medial SMA region (MNI305 peak: [8, 3, 52]). The thick black line represents the correlation time course within this cluster, with the red-shaded area highlighting its time span (p < 0.05, corrected). *Lower panel*: The right M1 elbow area

(MNI305 peak: [32, -20, 66]) and its correlation time course, which did not reach significance. **B:** Spearman's correlation coefficients (R) between 8-30 Hz periodic power and EMG inhibition in the SMA cluster (upper) and M1 elbow region (lower). Thin black lines indicate significant correlation effect ($p < 0.05$, corrected). **C:** Mediation analysis results showing the relationships between Beta power (independent variable), Gamma power (mediator), and EMG inhibition (dependent variable). Linear regression coefficients with the respective p-values are reported.

*p<0.05; **p<0.01; ***p<0.001

In contrast to the voluntary unloading condition, no significant positive correlation was observed under the imposed unloading condition between high-gamma power and the strength of the unloading reflex (EMG suppression) in the *Biceps brachii*.

To further assess the contribution of other brain regions to anticipatory inhibition via alpha and beta synchrony, we computed Spearman's rank correlations between periodic power (8-30 Hz) and EMG inhibition across sources in the right anticipatory motor network and subcortical structures (basal ganglia and cerebellum). The permutation cluster test revealed no significant correlation effect between EMG inhibition and alpha-beta band power in either cortical or subcortical regions.

SMA cluster-based analysis

Having identified the medial SMA cluster as the key cortical region where stronger EMG inhibition was linked to reduced high-gamma activity, we sought to test whether alpha- and/or beta-band rhythmic activity might mediate this inhibitory effect. Specifically, we

aimed to determine whether alpha-beta periodic power correlates with both the strength of EMG inhibition and the reduction in high-gamma power in the SMA cluster.

In each of the 10 vertices within the SMA cluster, we computed Spearman's rank correlations between alpha-beta band (8-30 Hz) periodic power and EMG inhibition across time (-0.25 to 0 s relative to unloading) to examine whether stronger alpha-beta power was associated with more prominent EMG inhibition. A one-sample, one-tailed permutation cluster test comparing correlations against zero revealed a significant negative correlation effect, peaking in the high-beta range (18-25 Hz) and spanning -0.228 to -0.018 s (Fig. 3B). Notably, this time window overlapped with the EMG inhibition calculation period (red dashed line, Fig. 3B) at 24-25 Hz, suggesting that high-beta activity may support optimal anticipatory inhibition in the *Biceps brachii*. Given the short latency between SMA stimulation and muscle response (mean MEP latency: 15.7 ms in Spieser et al., (2013); 22.6 ms in Entakli et al., (2014)), it is plausible that the observed late high-beta (24-25 Hz) effect reflects a direct inhibitory influence. By contrast, earlier lower-frequency correlations may be associated with preparatory beta-band synchronization supporting inhibitory communication. However, exploring this possibility lies beyond the scope of the current study.

To investigate the relationship between late high-beta and high-gamma activity within the SMA cluster, we computed partial Spearman's correlation coefficients at each cluster vertex between 24-25 Hz power and 90-130 Hz power, averaged over both frequency and the gamma correlation time window (-0.06 to -0.018 s; Fig. 3A), while controlling for broadband 1-130 Hz power to correct for shared variance from broadband fluctuations (Spaak et al., 2012). This approach revealed significantly negative individual correlation coefficients (one-sample t-test: $t = -7.16$, $p < 0.001$; Fig. S3B), indicating that stronger high-beta power was reliably linked to a more pronounced suppression of high-gamma power. A similar, albeit weaker, negative correlation was observed when periodic beta power (after removing the aperiodic component) was correlated with high-gamma power (one-sample t-test: $t = -2.17$, p

= 0.046). To test whether the observed beta-gamma correlation was specific to the high-beta range, we computed partial Spearman correlations between high-gamma power averaged over time and frequency (90-130 Hz; -0.06 to -0.018 s) and lower-frequency power across a broader time and frequency range (8-30 Hz; -0.25 to 0 s; Fig. S3A). As expected, significant correlations peaked at 25 Hz, but a secondary peak was observed at 9 Hz. However, because the 9 Hz effect was not linked to EMG inhibition (Fig. 3B), it likely reflects excitability fluctuations unrelated to anticipatory inhibition strength.

Since the relationship between EMG inhibition strength and reduced excitability was observed in the SMA, but not in M1, suggesting that the SMA mediates control over the *Biceps brachii* during voluntary unloading, we further examined whether correlations with EMG inhibition could be detected in the M1 elbow region for high-gamma power and for periodic alpha-beta power (8-30 Hz). The M1 coordinates for the left elbow area (*Biceps & Triceps brachii*) were derived from Talairach space (Lotze et al., 2000; Plow et al., 2010), converted to MNI305 space, and averaged to yield [32, -20, 66] in the right hemisphere. The M1 elbow region was defined as the peak vertex and its six adjacent vertices, forming a seven-vertex M1 elbow label (see Fig. 3A, lower panel). The permutation cluster test did not reveal a significant correlation between EMG inhibition and either high-gamma power or 8-30 Hz periodic power in this region.

Mediation analysis

A mediation analysis was conducted to examine whether the correlation between high-beta power and EMG inhibition in the SMA is mediated by high-gamma power reduction. To this end, data were extracted from the SMA cluster source showing the strongest correlation between high-gamma power and EMG inhibition. In the defined model, beta power was the

independent variable (X), EMG inhibition was the dependent variable (Y), and gamma power served as the mediator (M). The GAMs, referred to as models A, B, C, and C' (see Methods, *Mediation analysis* section), showed the following relationships: beta power predicted gamma power (*model A*: estimate (β) = -0.138, standard error (SE) = 0.027, 95% confidence interval (CI) = [-0.190,-0.085], t = -5.18, $p < 0.001$), gamma power predicted EMG inhibition (*model B*: β = 0.106, SE = 0.035, 95% CI = [0.037,0.175], t = 3.061, p = 0.002), beta power predicted EMG inhibition (*model C*: β = -0.069, SE = 0.025, 95% CI = [-0.120,-0.019], t = -2.725, p = 0.007), and beta power and gamma power together predicted EMG inhibition (*model C'*: beta power: β = -0.056, SE = 0.025, 95% CI = [-0.108,-0.005], t = -2.188, p = 0.029; gamma power: β = 0.092, SE = 0.035, 95% CI = [0.022,0.162], t = 2.609, p = 0.009).

The results of the mediation analysis are presented in Table 2, see also Fig. 3C. The analysis revealed a statistically significant mediation effect (Average Causal Mediation Effect, ACME) of gamma power on the relationship between beta power and EMG inhibition, as well as a significant total effect. However, the direct effect (Average Direct Effect, ADE) of beta power on EMG inhibition, after accounting for the mediator, was also significant. The proportion of the total effect of beta power on EMG inhibition that was explained by the mediator accounted for 18%, suggesting a partial mediation.

	Estimate (β)	95% CI	p-value
ACME	-0.013	[-0.02, 0.00]	0.006 **
ADE	-0.057	[-0.11, -0.01]	0.027 *
Total effect	-0.069	[-0.12, -0.02]	0.007 **
Proportion mediated	0.183	[0.04, 0.67]	0.013 **

Table 2. Results of the mediation analysis examining whether the relationship between high-beta power and EMG inhibition is mediated by high-gamma power. In this model, high-beta power (24-25 Hz) serves as the independent variable (X), EMG inhibition as the dependent variable (Y), and high-gamma power (90-130 Hz) as the mediator (M).

95% CI: 95% Confidence Interval; *ACME:* Average Causal Mediation Effect; *ADE:* Average Direct Effect.

*<0.05, **<0.01

Beta burst analysis

Since beta activity in the brain typically manifests as brief bursts rather than sustained rhythms (Little et al., 2019; Lundqvist et al., 2024), we sought to validate our findings on beta-mediated inhibition with burst analysis. Specifically, we examined whether trials containing beta bursts exhibit anticipatory *Biceps brachii* inhibition and high-gamma power suppression.

Beta bursts (13-30 Hz) were detected in the SMA cluster vertex showing the strongest correlation between high-gamma power and EMG inhibition. Among the detected bursts, only those centered around the time and frequency range of the late correlation effect between high-beta power and EMG inhibition were selected for further analysis (-0.077 to -0.018 s, and 22-28 Hz; Fig. 3B). This choice was motivated by the need to put constraints to select beta bursts potentially linked to anticipatory inhibition from those related to other processes. We assumed that inhibition-related beta bursts should occur close to the gamma-to-EMG inhibition correlation effect (18-60 ms before unloading; Fig. 3A) given the high conduction velocity, and approximately 15-25 ms (according to Spieser et al., 2013; Entakli et al., 2014) before the muscle inhibition interval, which corresponded to ~26 ms before

unloading. The 24-25 Hz beta correlation with EMG inhibition ($p < 0.05$) spanning -0.077 to -0.018 s (Fig. 3B) overlapped with the gamma correlation effect and reasonably preceded the muscle inhibition interval. We therefore constrained burst detection to this interval to capture only bursts that were closely time-locked to the inhibition-related effects. The frequency window was selected based on the peak frequency within the preselected time interval, which corresponded to 25 Hz. Considering the likely imprecision of standard time-frequency decomposition for asymmetric signals (Jones, 2016; Cole and Voytek, 2019), we allowed a broader frequency range for burst selection, spanning ±3 Hz around the 25 Hz peak. This selection also aimed to exclude the effect around 19 Hz (Fig. 3B), which lacked temporal precision, unlike the 24-25 Hz effect that was confined to the time of inhibition.

The percentage of trials containing the selected beta bursts was low, with a mean ± SD of 11.6 ± 1.9% per participant. The absolute number of trials with bursts was 10.1 ± 1.78 (mean ± SD). Notably, the number of trials with bursts remained consistent when the time-frequency signal was extracted from the 10 vertices of the medial SMA cluster and averaged for burst detection.

Beta bursts and EMG inhibition

The results above demonstrate that greater EMG inhibition is associated with increased high-beta power in the SMA. However, given that beta activity occurs in transient bursts, we suggested that the presence of bursts could more effectively predict the timing of anticipatory inhibition than beta power alone. To test this, we averaged baseline-corrected EMG power across trials containing bursts for each subject. A permutation cluster test comparing this averaged EMG power to zero revealed a significant decrease in EMG activity during burst trials, peaking at -0.026 s relative to unloading (t_{max}=3.92, $p = 0.009$; Fig. 4A), which coincides with the behaviourally defined optimal *Biceps brachii* inhibition window (see

Results, *Behavioural data* section). In contrast, selecting an equal number of trials based on the highest beta power within the time-frequency window used for burst detection yielded no significant effect ($p > 0.18$). These findings, consistent with earlier work (Little et al., 2019), suggest that the occurrence of a burst, rather than its amplitude, can better reflect its functional impact. Notably, another study found a link between burst power and movement velocity (Torrecillos et al., 2018), suggesting that burst power may still be a behaviourally relevant metric depending on the behaviour studied or time window.

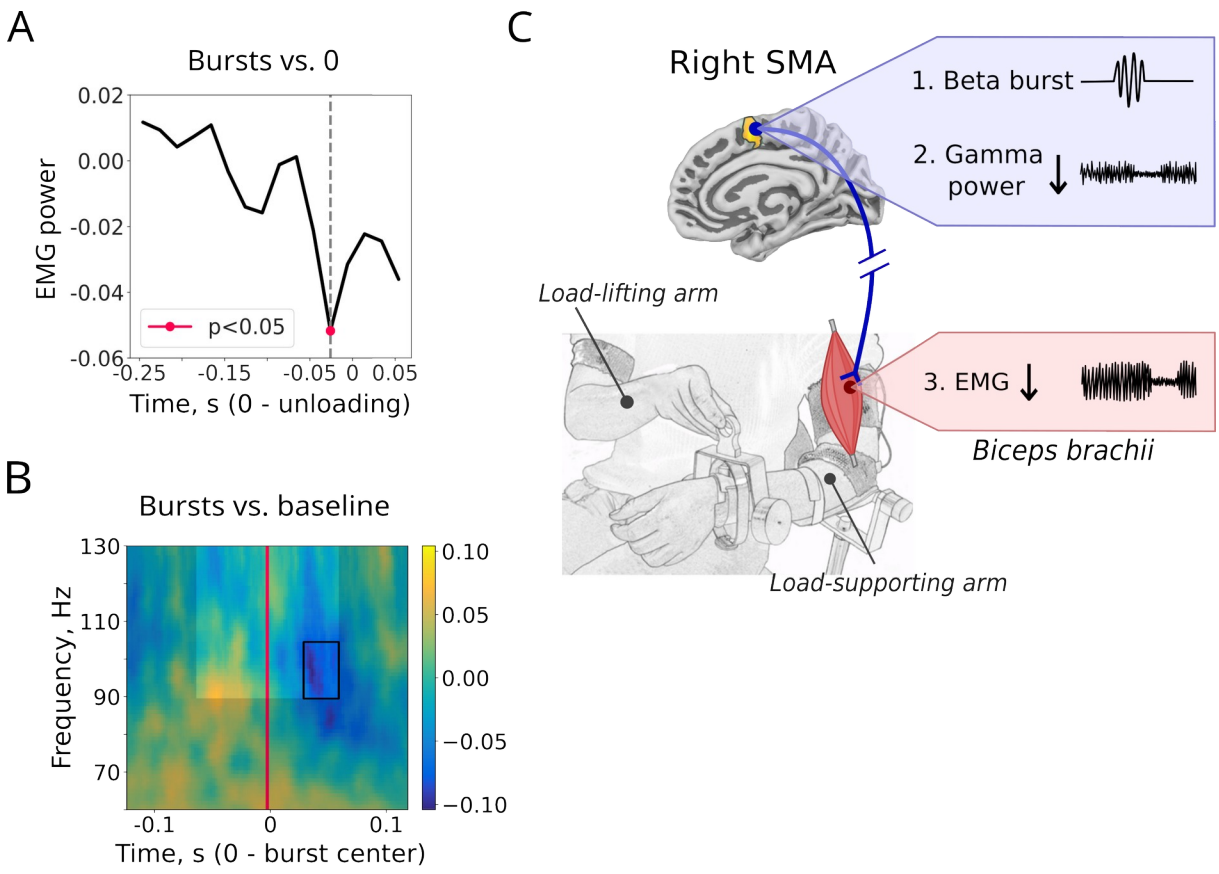

Figure 4. Beta burst analysis results. **A:** Baseline-corrected EMG power averaged across SMA burst trials. Notably, the timing of the most pronounced EMG suppression coincides with the behaviourally defined optimal *Biceps brachii* inhibition window. **B:** Time-frequency contrast of gamma power between SMA burst and no-burst trials. Bright rectangle indicates the analysis window, and thin black lines mark time-frequency points showing significant

contrast effects ($p < 0.05$, corrected). **C:** Schematic illustrating the proposed sequence of neural events during voluntary load-lifting leading to anticipatory inhibition of the postural elbow flexor, the *Biceps brachii*. An inhibitory beta burst (22-28 Hz) in the SMA contralateral to the muscle (1) is followed by a reduction in excitability in this area, reflected by suppression of high-gamma (90-130 Hz) activity (2), which in turn leads to inhibition of the *Biceps brachii* (3). This inhibition reaches its maximum effect prior to unloading, stabilizing posture.

Beta bursts and gamma power

As described above, high-beta power negatively correlated with high-gamma activity in the SMA cluster region (see *SMA cluster-based analysis* section*;* Fig. S3B). However, since beta activity occurs in bursts, we further tested whether the presence of beta bursts was associated with high-gamma power suppression within the same trials. A permutation cluster test confirmed a significant reduction in high-gamma power (90-130 Hz) in trials with beta bursts compared to baseline trials (Fig. 4B): in burst-centered data, high-gamma power decreased most prominently between 0.026 and 0.05 s following the burst center ($T_{max} = -4.96$, $p_{min} = 0.032$).

Discussion

In this study, we investigated the neural mechanisms underlying anticipatory inhibition of the elbow flexor, the *Biceps brachii*, in the load-supporting arm, which counteracts forearm destabilization during voluntary load-lifting. Stronger muscle inhibition was linked to reduced excitability, indexed by lower high-gamma power, in the contralateral SMA, and to increased high-beta power, with gamma suppression partially mediating this relationship. Notably, the presence of beta bursts (22-28 Hz) in the SMA was a stronger predictor of timed inhibition than beta power alone. Together, our findings suggest that, in anticipation of load-lifting, high-frequency beta bursts inhibit the SMA, leading to suppression of the contralateral *Biceps brachii* and stabilization of posture (Fig. 4C).

During voluntary unloading, lifting a load induces a change in force, which is counteracted by timed anticipatory inhibition restoring equilibrium. The precise timing of this inhibition is essential for efficient bimanual coordination (Hugon et al., 1982; Viallet et al., 1987) and is altered in Parkinson's disease (Viallet et al., 1987), autism spectrum disorders (Schmitz et al., 2003), and other developmental motor-related conditions (Jover et al., 2006, 2010). In adults, anticipatory inhibition is closely time-locked to the same muscle activation in the load-lifting arm, suggesting a central timing mechanism coordinating both arms (Paulignan et al., 1989; Massion, 1992). However, developmental studies reveal that this precise temporal coordination is acquired gradually during childhood (Schmitz et al., 2002; Barlaam et al., 2012). Bolzoni et al. (2015) further demonstrated that APA can be selectively influenced through modulation of SMA activity without affecting voluntary movement. These findings suggest that APA are governed by a separate control mechanism, which integrates movement parameters and predicted postural disturbances to generate timely

adjustments in muscle activity. To investigate the mechanism of anticipatory muscle inhibition, a core component of APA in the BLLT, we therefore focused on the right-hemispheric network contralateral to the postural arm where APA occur.

Although anticipatory inhibition is well-developed in adults, its latency still exhibits some variability (Barlaam et al., 2012). We observed that optimal forearm stabilization is achieved when *Biceps brachii* inhibition precedes the onset of unloading by 26 ± 15 ms, consistent with previously reported adult latencies (25 ms: Dufossé et al. (1985); 32 ms: Barlaam et al. (2012)).

A potential association between elbow flexor activity and M1 excitability during BLLT was previously explored by (Kazennikov et al., 2005, 2006). Using transcranial magnetic stimulation (TMS), they showed reduced M1 excitability, measured by motor evoked potentials (MEPs), during anticipatory *Biceps brachii* inhibition. However, a similar MEP-EMG relationship was also observed under control conditions, suggesting that the effect was not specific to APA. In our study, we assessed high-gamma (90-130 Hz) power, which closely correlates with neural spiking (Ray et al., 2008; Lundqvist et al., 2016; Riehle et al., 2018; Brazhnik et al., 2021), as a proxy for excitability. Surprisingly, we found no association between *Biceps brachii* inhibition and M1 excitability. However, stronger muscle inhibition was correlated with reduced excitability in the medial SMA – a relationship specific to the voluntary unloading, as it did not appear in the control condition where anticipating load release was not possible.

The involvement of the SMA in BLLT has been consistently demonstrated in MEG and fMRI studies (Schmitz et al., 2005; Ng et al., 2011, 2013b). APA impairments following contralateral SMA lesions (Viallet et al., 1992) led authors to propose that the SMA contributes to gating postural stabilization circuits. The observed link between anticipatory inhibition and SMA suppression aligns with and extends this proposal, suggesting that the SMA exerts direct control over the postural load-supporting elbow flexors during voluntary

load-lifting. This control appears to be attenuated in anticipation of force changes, reflected in SMA and muscle inhibition. Our results therefore support the previous speculation by Ng et al. (2013b) that the SMA, rather than M1, mediates APA via direct corticospinal projections. This interpretation is plausible, as the SMA displays precise somatotopic organization (He et al., 1995; Strother et al., 2012) and has corticospinal projections about half as extensive as those of M1 (Dum and Strick, 1991). Additionally, TMS stimulation of the SMA during motor tasks in humans evokes arm muscle MEPs similar in latency and amplitude to those from M1 (Spieser et al., 2013; Entakli et al., 2014). These findings indicate that the SMA can exert direct and precise control over arm muscles.

The assessment of neural excitability through high-gamma activity during a motor task using a non-invasive technique may raise concerns about potential contamination from myogenic artifacts (Whitham et al., 2008; Muthukumaraswamy, 2013). We, however, argue that this is unlikely to affect our results. First, *Biceps brachii* inhibition was associated with decreased, rather than increased, high-gamma power, with the effect confined to the SMA on the medial surface, where tonic muscle contamination is expected to be low. Second, small head motion (<1 cm) and the absence of visible movement during the anticipatory period suggest minimal phasic EMG contamination. Combined with source localization based on spatial filtering, which reduces broadband myogenic gamma artifacts (Hipp and Siegel, 2013; Manyukhina et al., 2022), we argue that the observed correlation between muscle inhibition and high-gamma power reflects a genuine neural process.

In humans, SMA-originating corticospinal projections are more prominent than in non-human primates (Maier et al., 2002), which may have evolved to facilitate anticipatory control during complex hand movements (Chen et al., 2013). Such SMA-mediated hand muscle control, supported by beta-band coherence, has been demonstrated in a task requiring precise, time-predictable force production in humans (Chen et al., 2013; Spieser et al., 2013; Entakli et al., 2014). Similarly, forearm stabilization during voluntary unloading may involve

partial, selective control of the elbow flexors by the SMA, the release of which facilitates a smooth transition to a new postural state. We propose that this release is associated with SMA suppression, mediated by beta bursts. Whether this mechanism is specific to the optimal inhibition time interval, rather than to earlier or later times, requires further investigation.

Beta-band activity has been extensively implicated in motor control, particularly through its established role in maintaining and adjusting muscle force production according to task demands (Peng et al., 2024). Yet, the mechanisms by which beta activity mediates cortex-muscle interactions, ultimately shaping behavior, remain poorly understood (Khanna and Carmena, 2017; Peng et al., 2024). Although traditionally considered a sustained rhythm, increasing evidence indicates that beta activity is organized in transient oscillatory events – bursts (Lundqvist et al., 2024), and considering the true temporal structure of brain dynamics may advance our understanding of the neural mechanisms linking brain and muscle activity. In particular, cortical beta bursts have been shown to elicit time-locked bursts of similar duration and rate in contracting muscles (Bräcklein et al., 2022). Beta bursts have also been reported to establish synchrony between muscles during static postures (Simpson et al., 2024) and to promote cortico-muscular synchrony during sustained isometric muscle contractions (Echeverria-Altuna et al., 2022).

Another line of evidence links beta activity, and particularly beta bursts, to action slowing or cancellation: later burst timing is consistently associated with delayed responses (Khanna and Carmena, 2017; Little et al., 2019) and slower stopping (Hannah et al., 2020; Jana et al., 2020). This suggests that beta bursts can exert an inhibitory influence on muscles, yet the neural mechanisms underlying this effect remain unexplored. Our results align with this evidence and suggest a mechanism through which a beta burst suppresses muscle activity during natural posture-movement coordination. Specifically, our results suggest that during load support, inhibitory beta bursts arising in the SMA shortly before load-lifting suppress

SMA activity, thereby releasing its control over the *Biceps brachii* and producing EMG-measured muscle inhibition. The latency of the observed beta-to-muscle inhibition correlation in the SMA (~20 ms; Fig. 3B) closely matches previously reported MEP latencies following SMA stimulation (15.7 ms, Spieser et al. (2013); 22.6 ms, Entakli et al. (2014)). Notably, we found that the beta effect on muscle inhibition was partially mediated by reduced high-gamma activity, supporting the proposition that, during posture-movement coordination, beta-related anticipatory inhibition is likely achieved through SMA suppression. While, as discussed above, the role of beta is not limited to inhibition, our findings are consistent with prior reports of an inverse relationship between beta and high-gamma/spiking activity in sensorimotor areas (Ray et al., 2008; Lundqvist et al., 2016; Riehle et al., 2018), corroborating their opposing functional roles – excitatory for high-gamma and inhibitory for beta (Ray and Maunsell, 2011; Lundqvist et al., 2024).

Alpha-band activity was another candidate for mediating anticipatory inhibition in the BLLT, however, we did not find evidence in favor of this. Previous studies linking alpha activity to motor control primarily describe its role in action withholding (Bönstrup et al., 2015; Köster and Meyer, 2023), consistent with the proposed “gating by inhibition” hypothesis for alpha oscillations (Jensen and Mazaheri, 2010). Alpha activity may therefore gate the selection of appropriate motor commands, rather than shaping the precision of ongoing muscle control, which is instead attributed to beta-band activity. Alternatively, while transient beta activity may mediate temporally precise, short-lived muscle inhibition, alpha activity, by creating a window of excitability, could influence the temporal profile of this inhibition lengthening its duration, or mediate longer-lasting muscle suppression, as proposed by Bonnefond and Jensen (2025).

While our findings indicate that the SMA mediates the core events underlying anticipatory *Biceps brachii* inhibition during the BLLT, the circuitry conveying inhibitory bursts to the SMA remains unstudied. We found no correlation between alpha-beta power and

anticipatory inhibition in the examined cortical and subcortical right-hemispheric network, suggesting that inhibition strength may rely primarily on local SMA computations, whereas other regions may contribute to generating the APA command without directly influencing inhibition strength. Moreover, burst involvement might obscure the relationship, as burst occurrence can be a stronger behavioural predictor than beta power, as shown in our data (Fig. 4A) and previous research (Little et al., 2019). To partially address the limitations arising from the event-like nature of beta activity (Lundqvist et al., 2024), we performed a directed connectivity analysis on SMA beta bursts (see Supplementary Materials for details; Figs S4,S5). While limitations in spatial resolution and trial count prevent this analysis from conclusively identifying the full network giving rise to SMA beta bursts, our exploratory findings allowed us to speculate on potential sources. Future research would benefit from further investigation of the network underlying anticipatory inhibition, taking intrinsic neural dynamics into account to better elucidate the mechanisms governing its generation and timing.

One limitation of this study is the inability to track individual inhibitory events in the *Biceps brachii*, which, together with a sample size limited to sixteen participants, constrains our capacity to assess the involvement of subcortical structures – specifically the basal ganglia and cerebellum – in anticipatory inhibition, given the lower signal-to-noise ratio for deep MEG sources (Attal and Schwartz, 2013). Furthermore, while burst selection within predefined time-frequency windows and burst-centered analysis addressed some challenges, the variability in burst waveforms and their temporal dynamics (Szul et al., 2023) calls for novel methods linking burst features to relevant events. Such approaches would be particularly valuable for detecting transient network synchrony linked to different functional roles (Lundqvist et al., 2024).

In conclusion, our findings reveal a cortical mechanism for anticipatory inhibition in the Bimanual Load-Lifting Task. We demonstrate that shortly before load-lifting, high-frequency beta bursts in the SMA inhibit the postural elbow flexor, the *Biceps brachii*. This process is mediated by SMA suppression, potentially releasing its control over the muscle and subsequently leading to *Biceps brachii* inhibition. These data highlight a specific role of the SMA in anticipatory postural control and suggest that beta activity, particularly in bursts, can directly govern inhibitory control of muscle function.

Conflict of interest

The authors declare no conflict of interest.

Acknowledgments

The authors would like to thank Jérôme Prado, Franck Lamberton, and Sarah Le Diagon for their valuable contributions to this study, as well as the staff of CERMEP–Imagerie du Vivant for their helpful assistance with data collection.

Funding

This study was supported by funding from the French National Research Agency: ANR SaMenta ASD-BARN (ANR-12-SAMA-015-01), LABEX CORTEX (ANR-11-LABX-0042) of Université de Lyon, within the program “Investissements d'Avenir” (ANR-11-IDEX-0007). Viktoriya Manyukhina was funded by a scholarship from the French Ministry of Research and by the Fondation pour la Recherche Médicale (FRM, FDT202504020439).

References

Attal Y, Schwartz D (2013) Assessment of Subcortical Source Localization Using Deep Brain Activity Imaging Model with Minimum Norm Operators: A MEG Study Barnes GR, ed. PLoS ONE 8:e59856.

Barlaam F, Descoins M, Bertrand O, Hasbroucq T, Vidal F, Assaiante C, Schmitz C (2011) Time–Frequency and ERP Analyses of EEG to Characterize Anticipatory Postural Adjustments in a Bimanual Load-Lifting Task. Frontiers in Human Neuroscience 5.

Barlaam F, Fortin C, Vaugoyeau M, Schmitz C, Assaiante C (2012) Development of action representation during adolescence as assessed from anticipatory control in a bimanual load-lifting task. Neuroscience 221:56–68.

Barlaam F, Fortin C, Vaugoyeau M, Schmitz C, Assaiante C (2018) Mu-oscillation changes related to the development of anticipatory postural control in children and adolescents. Journal of Neurophysiology 120:129–138.

Bolzoni F, Bruttini C, Esposti R, Castellani C, Cavallari P (2015) Transcranial direct current stimulation of SMA modulates anticipatory postural adjustments without affecting the primary movement. Behavioural Brain Research 291:407–413.

Bonnefond M, Jensen O (2025) The role of alpha oscillations in resisting distraction. Trends in Cognitive Sciences 29:368–379.

Bönstrup M, Hagemann J, Gerloff C, Sauseng P, Hummel FC (2015) Alpha oscillatory correlates of motor inhibition in the aged brain. Front Aging Neurosci 7.

Borgomaneri S, Serio G, Battaglia S (2020) Please, don’t do it! Fifteen years of progress of non-invasive brain stimulation in action inhibition. Cortex 132:404–422.

Bräcklein M, Barsakcioglu DY, Del Vecchio A, Ibáñez J, Farina D (2022) Reading and Modulating Cortical β Bursts from Motor Unit Spiking Activity. J Neurosci 42:3611.

Brazhnik E, Novikov N, McCoy AJ, Ilieva NM, Ghraib MW, Walters JR (2021) Early decreases in cortical mid-gamma peaks coincide with the onset of motor deficits and precede exaggerated beta build-up in rat models for Parkinson's disease. Neurobiology of Disease 155:105393.

Chen S, Entakli J, Bonnard M, Berton E, De Graaf JB (2013) Functional Corticospinal Projections from Human Supplementary Motor Area Revealed by Corticomuscular Coherence during Precise Grip Force Control Gribble PL, ed. PLoS ONE 8:e60291.

Cole S, Voytek B (2019) Cycle-by-cycle analysis of neural oscillations. Journal of Neurophysiology 122:849–861.

Di Rienzo F, Barlaam F, Daligault S, Delpuech C, Roy AC, Bertrand O, Jerbi K, Schmitz C (2019) Tracking the acquisition of anticipatory postural adjustments during a bimanual load-lifting task: A MEG study. Human Brain Mapping 40:2955–2966.

Donoghue T, Haller M, Peterson EJ, Varma P, Sebastian P, Gao R, Noto T, Lara AH, Wallis JD, Knight RT, Shestyuk A, Voytek B (2020) Parameterizing neural power spectra into periodic and aperiodic components. Nat Neurosci 23:1655–1665.

Dufossé M, Hugon M, Massion J (1985) Postural forearm changes induced by predictable in time or voluntary triggered unloading in man. Experimental Brain Research 60:330–334.

Dum R, Strick P (1991) The origin of corticospinal projections from the premotor areas in the frontal lobe. J Neurosci 11:667–689.

Entakli J, Bonnard M, Chen S, Berton E, De Graaf JB (2014) TMS reveals a direct influence of spinal projections from human SMAp on precise force production. Eur J of Neuroscience 39:132–140.

Fischl B, Salat DH, Busa E, Albert M, Dieterich M, Haselgrove C, Van Der Kouwe A, Killiany R, Kennedy D, Klaveness S, Montillo A, Makris N, Rosen B, Dale AM (2002) Whole Brain Segmentation. Neuron 33:341–355.

Glasser MF, Coalson TS, Robinson EC, Hacker CD, Harwell J, Yacoub E, Ugurbil K, Andersson J, Beckmann CF, Jenkinson M, Smith SM, Van Essen DC (2016) A multi-modal parcellation of human cerebral cortex. Nature 536:171–178.

Gramfort A, Luessi M, Larson E, Engemann DA, Strohmeier D, Brodbeck C, Goj R, Jas M, Brooks T, Parkkonen L, Hämäläinen M (2013) MEG and EEG data analysis with MNE-Python. Front Neurosci 7:267.

Hannah R, Muralidharan V, Sundby KK, Aron AR (2020) Temporally-precise disruption of prefrontal cortex informed by the timing of beta bursts impairs human action-stopping. NeuroImage 222:117222.

He S, Dum R, Strick P (1995) Topographic organization of corticospinal projections from the frontal lobe: motor areas on the medial surface of the hemisphere. J Neurosci 15:3284–3306.

Hipp JF, Siegel M (2013) Dissociating neuronal gamma-band activity from cranial and ocular muscle activity in EEG. Front Hum Neurosci 7.

Hugon M, Massion J, Wiesendanger M (1982) Anticipatory postural changes induced by active unloading and comparison with passive unloading in man. Pflugers Arch 393:292–296.

Jana S, Hannah R, Muralidharan V, Aron AR (2020) Temporal cascade of frontal, motor and muscle processes underlying human action-stopping. eLife 9:e50371.

Jensen O, Mazaheri A (2010) Shaping Functional Architecture by Oscillatory Alpha Activity: Gating by Inhibition. Front Hum Neurosci 4.

Jones SR (2016) When brain rhythms aren't 'rhythmic': implication for their mechanisms and meaning. Current Opinion in Neurobiology 40:72–80.

Jover M, Schmitz C, Bosdure E, Chabrol B, Assaiante C (2006) Anticipatory postural adjustments in a bimanual load-lifting task in children with Duchenne muscular dystrophy. Neuroscience Letters 403:271–275.

Jover M, Schmitz C, Centelles L, Chabrol B, Assaiante C (2010) Anticipatory postural adjustments in a bimanual load-lifting task in children with developmental coordination disorder. Develop Med Child Neuro 52:850–855.

Kazennikov O, Solopova I, Talis V, Grishin A, Ioffe M (2005) TMS-responses during anticipatory postural adjustment in bimanual unloading in humans. Neuroscience Letters 383:246–250.

Kazennikov OV, Solopova IA, Talis VL, Grishin AA, Ioffe ME (2006) Involvement of the Motor Cortex in the Bimanual Unloading Reaction: A Transcranial Magnetic Stimulation Study. Neurosci Behav Physiol 36:177–183.

Khanna P, Carmena JM (2017) Beta band oscillations in motor cortex reflect neural population signals that delay movement onset. eLife 6:e24573.

Köster M, Meyer M (2023) Down and up! Does the mu rhythm index a gating mechanism in the developing motor system? Developmental Cognitive Neuroscience 60:101239.

Little S, Bonaiuto J, Barnes G, Bestmann S (2019) Human motor cortical beta bursts relate to movement planning and response errors. PLoS Biol 17:e3000479.

Lotze M, Erb M, Flor H, Huelsmann E, Godde B, Grodd W (2000) fMRI Evaluation of Somatotopic Representation in Human Primary Motor Cortex. NeuroImage 11:473–481.

Lundqvist M, Miller EK, Nordmark J, Liljefors J, Herman P (2024) Beta: bursts of cognition. Trends in Cognitive Sciences 28:662–676.

Lundqvist M, Rose J, Herman P, Brincat SL, Buschman TJ, Miller EK (2016) Gamma and Beta Bursts Underlie Working Memory. Neuron 90:152–164.

Maier MA, Armand J, Kirkwood PA, Yang H-W, Davis JN, Lemon RN (2002) Differences in the corticospinal projection from primary motor cortex and supplementary motor area to macaque upper limb motoneurons: an anatomical and electrophysiological study. Cereb Cortex 12:281–296.

Manyukhina VO, Prokofyev AO, Galuta IA, Goiaeva DE, Obukhova TS, Schneiderman JF, Altukhov DI, Stroganova TA, Orekhova EV (2022) Globally elevated excitation–inhibition ratio in children with autism spectrum disorder and below-average intelligence. Molecular Autism 13:20.

Massion J (1992) Movement, posture and equilibrium: Interaction and coordination. Progress in Neurobiology 38:35–56.

Massion J, Ioffe M, Schmitz C, Viallet F, Gantcheva R (1999) Acquisition of anticipatory postural adjustments in a bimanual load-lifting task: normal and pathological aspects. Experimental Brain Research 128:229–235.

Moca VV, Bârzan H, Nagy-Dăbâcan A, Mureşan RC (2021) Time-frequency super-resolution with superlets. Nat Commun 12:337.

Murthy VN, Fetz EE (1996) Oscillatory activity in sensorimotor cortex of awake monkeys: synchronization of local field potentials and relation to behavior. Journal of Neurophysiology 76:3949–3967.

Muthukumaraswamy SD (2013) High-frequency brain activity and muscle artifacts in MEG/EEG: a review and recommendations. Front Hum Neurosci 7.

Ng THB, Sowman PF, Brock J, Johnson BW (2011) Premovement brain activity in a bimanual load-lifting task. Exp Brain Res 208:189–201.

Ng THB, Sowman PF, Brock J, Johnson BW (2013a) Neuromagnetic brain activity associated with anticipatory postural adjustments for bimanual load lifting. NeuroImage 66:343–352.

Ng THB, Sowman PF, Brock J, Johnson BW (2013b) Neuromagnetic imaging reveals timing of volitional and anticipatory motor control in bimanual load lifting. Behavioural Brain Research 247:182–192.

Oldfield RC (1971) The assessment and analysis of handedness: the Edinburgh inventory. Neuropsychologia 9:97–113.

Paulignan Y, Dufossé M, Hugon M, Massion J (1989) Acquisition of co-ordination between posture and movement in a bimanual task. Exp Brain Res 77:337–348.

Peng J, Zikereya T, Shao Z, Shi K (2024) The neuromechanical of Beta-band corticomuscular coupling within the human motor system. Front Neurosci 18:1441002.

Picazio S, Veniero D, Ponzo V, Caltagirone C, Gross J, Thut G, Koch G (2014) Prefrontal Control over Motor Cortex Cycles at Beta Frequency during Movement Inhibition. Current Biology 24:2940–2945.

Plow EB, Arora P, Pline MA, Binenstock MT, Carey JR (2010) Within-limb somatotopy in primary motor cortex – revealed using fMRI. Cortex 46:310–321.

Ray S, Crone NE, Niebur E, Franaszczuk PJ, Hsiao SS (2008) Neural Correlates of High-Gamma Oscillations (60–200 Hz) in Macaque Local Field Potentials and Their Potential Implications in Electrocorticography. J Neurosci 28:11526–11536.

Ray S, Maunsell JHR (2011) Different Origins of Gamma Rhythm and High-Gamma Activity in Macaque Visual Cortex Ungerleider L, ed. PLoS Biol 9:e1000610.

Riehle A, Brochier T, Nawrot M, Grün S (2018) Behavioral Context Determines Network State and Variability Dynamics in Monkey Motor Cortex. Front Neural Circuits 12:52.

Schaum M, Pinzuti E, Sebastian A, Lieb K, Fries P, Mobascher A, Jung P, Wibral M, Tüscher O (2020) Cortical network mechanisms of response inhibition.

Schmitz C, Jenmalm P, Ehrsson HH, Forssberg H (2005) Brain Activity During Predictable and Unpredictable Weight Changes When Lifting Objects. Journal of Neurophysiology 93:1498–1509.

Schmitz C, Martin N, Assaiante C (2002) Building anticipatory postural adjustment during childhood: a kinematic and electromyographic analysis of unloading in children from 4 to 8 years of age. Experimental Brain Research 142:354–364.

Schmitz C, Martineau J, Barthélémy C, Assaiante C (2003) Motor control and children with

autism: deficit of anticipatory function? Neuroscience Letters 348:17–20.

Simpson TG, Godfrey W, Torrecillos F, He S, Herz DM, Oswal A, Muthuraman M, Pogosyan A, Tan H (2024) Cortical beta oscillations help synchronise muscles during static posture holding in healthy motor control. NeuroImage 298:120774.

Spaak E, Bonnefond M, Maier A, Leopold DA, Jensen O (2012) Layer-Specific Entrainment of Gamma-Band Neural Activity by the Alpha Rhythm in Monkey Visual Cortex. Current Biology 22:2313–2318.

Spieser L, Aubert S, Bonnard M (2013) Involvement of SMAp in the intention-related long latency stretch reflex modulation: A TMS study. Neuroscience 246:329–341.

Strother L, Medendorp WP, Coros AM, Vilis T (2012) Double representation of the wrist and elbow in human motor cortex. Eur J of Neuroscience 36:3291–3298.

Suffczynski P, Crone NE, Franaszczuk PJ (2014) Afferent inputs to cortical fast-spiking interneurons organize pyramidal cell network oscillations at high-gamma frequencies (60–200 Hz). Journal of Neurophysiology 112:3001–3011.

Szul MJ, Papadopoulos S, Alavizadeh S, Daligaut S, Schwartz D, Mattout J, Bonaiuto JJ (2023) Diverse beta burst waveform motifs characterize movement-related cortical dynamics. Progress in Neurobiology 228:102490.

Torrecillos F, Tinkhauser G, Fischer P, Green AL, Aziz TZ, Foltynie T, Limousin P, Zrinzo L, Ashkan K, Brown P, Tan H (2018) Modulation of Beta Bursts in the Subthalamic Nucleus Predicts Motor Performance. J Neurosci 38:8905–8917.

Viallet F, Massion J, Massarino R, Khalil R (1987) Performance of a bimanual load-lifting task by parkinsonian patients. Journal of Neurology, Neurosurgery & Psychiatry

50:1274–1283.

Viallet F, Massion J, Massarino R, Khalil R (1992) Coordination between posture and movement in a bimanual load lifting task: putative role of a medial frontal region including the supplementary motor area. Exp Brain Res 88.

Whitham EM, Lewis T, Pope KJ, Fitzgibbon SP, Clark CR, Loveless S, DeLosAngeles D, Wallace AK, Broberg M, Willoughby JO (2008) Thinking activates EMG in scalp electrical recordings. Clinical Neurophysiology 119:1166–1175.

Yazdan-Shahmorad A, Kipke DR, Lehmkuhle MJ (2013) High gamma power in ECoG reflects cortical electrical stimulation effects on unit activity in layers V/VI. J Neural Eng 10:066002.

Figure legends

Figure 1. Estimation of elbow deflection parameters and their expected relationship with *Biceps brachii* inhibition timing. **A:** Schematic illustration of three primary possible scenarios for *Biceps brachii* inhibition timing and its hypothetical impact on elbow rotation. See Methods (*Estimation of the EMG inhibition* section) for details. **B:** Single-trial examples aligned to unloading onset (time = 0), schematically illustrating the amplitudes of Peak Elbow Rotation and Elbow Rotation Decline. Values are presented as percentages of elbow deflection during voluntary unloading relative to the individual maximum, estimated as the median peak elbow rotation in the imposed condition.

Figure 2. Behavioural analysis results. Data in panels **A** and **C** are aligned to unloading onset (time = 0). **A:** Standardized elbow rotation and *Biceps brachii* EMG. Group means (black line) and SD (gray shading) are shown, with colored arrows indicating the amplitudes of behavioural measures: Elbow Rotation Decline (green), Peak Elbow Rotation (purple), and EMG inhibition (blue). **B:** Participant-wise mean (dots) and SD (whiskers) values for each measure, with boxplots indicating between-subject variability. The red line marks the median, box edges show quartiles (Q1 and Q3), and whiskers extend to 1.5 times the interquartile range. **C:** Group-averaged R^2 values from linear regression models computed at each time point (dependent variable: EMG power; independent variables: Peak Elbow Rotation, Elbow Rotation Decline). Red markers and gray dashed lines denote time points where the relationship between EMG inhibition and elbow rotation parameters reached significance.

Figure 3. Neural correlates of EMG inhibition and mediation analysis. Data in panels **A** and **B** are aligned to unloading onset (time = 0). **A:** *Upper panel:* A cluster-level significant correlation effect between high-gamma power (90-130 Hz) and EMG inhibition (30 ms window centered on -0.026 s, indicated by red dashed lines) with the strongest effect observed in the medial SMA region (MNI305 peak: [8, 3, 52]). The thick black line represents the correlation time course within this cluster, with the red-shaded area highlighting its time span ($p < 0.05$, corrected). *Lower panel*: The right M1 elbow area (MNI305 peak: [32, -20, 66]) and its correlation time course, which did not reach significance. **B:** Spearman's correlation coefficients (R) between 8-30 Hz periodic power and EMG inhibition in the SMA cluster (upper) and M1 elbow region (lower). Thin black lines indicate significant correlation effect ($p < 0.05$, corrected). **C:** Mediation analysis results showing the relationships between Beta power (independent variable), Gamma power (mediator), and EMG inhibition (dependent variable). Linear regression coefficients with the respective p-values are reported.

*p<0.05; **p<0.01; ***p<0.001

Figure 4. Beta burst analysis results. **A:** Baseline-corrected EMG power averaged across SMA burst trials. Notably, the timing of the most pronounced EMG suppression coincides with the behaviourally defined optimal *Biceps brachii* inhibition window. **B:** Time-frequency contrast of gamma power between SMA burst and no-burst trials. Bright rectangle indicates the analysis window, and thin black lines mark time-frequency points showing significant contrast effects ($p < 0.05$, corrected). **C:** Schematic illustrating the proposed sequence of neural events during voluntary load-lifting leading to anticipatory inhibition of the postural elbow flexor, the *Biceps brachii*. An inhibitory beta burst (22-28 Hz) in the SMA contralateral to the muscle (1) is followed by a reduction in excitability in this area, reflected by suppression of high-gamma (90-130 Hz) activity (2), which in turn leads to inhibition of the *Biceps brachii* (3). This inhibition reaches its maximum effect prior to unloading, stabilizing posture.